2007 IEEE International Conference on
Robotics and Automation
Roma, Italy, 10-14 April 2007

A Practical Redundancy Resolution for 7 DOF Redundant Manipulators with Joint Limits

Masayuki Shimizu, Woo-Keun Yoon, and Kosei Kitagaki

Intelligent Systems Research Institute
National Institute of Advanced Industrial Science and Technology
1-1-1, Umezono, Tsukuba, Ibaraki 305-8568, JAPAN
{*masayuki.shimizu, wk.yoon, k.kitagaki*}*@aist.go.jp*

***Abstract*— This paper proposes a practical redundancy resolution for 7 DOF redundant manipulators with joint limits. The primary concern of the paper is how to resolve the redundancy in the global configuration space when the movable joint angles are considerably restricted. First, a parameterized inverse kinematic solution for a 7 DOF manipulator model is derived. Second, how the joint limits affect the inverse kinematic solution is examined to explicitly identify the feasible solution under the joint limits. Then, an analytical redundancy resolution method for avoiding the joint limits is developed. Finally, kinematic simulations show that the method is effective for avoiding the joint limits as well as expanding the reachable region of the manipulator's tip.**

I. INTRODUCTION

This paper addresses the inverse kinematic problem for 7 degrees of freedom (DOF) redundant manipulators. Since a 7 DOF manipulator has an extra DOF inside the manipulator structure, an infinite number of inverse kinematic solutions are possible. To control the manipulator, a single solution has to be chosen from them. The problem of selecting one solution is conventionally referred to as *redundancy resolution*.

So far, a variety of redundancy resolution methods have been proposed. Most of them resolve the redundancy by optimizing a cost function at each moment [1]. It has been shown that various subtasks, such as manipulability enhancement [2], torque optimization [3], and obstacle avoidance [4], can be achieved with an appropriate cost function. However, these methods solve the inverse kinematic problem in the velocity domain based on the linearized first order instantaneous kinematic relation between tip velocities and joint velocities, which is characterized by a *Jacobian matrix*. Since the Jacobian-based methods provide only velocity solutions, the absolute tip pose (position and orientation) as well as repeatability in tracking closed trajectories are not guaranteed [5].

In contrast, redundancy resolution methods in the position domain have been proposed [6] [7]. In these methods, the inverse kinematic problem is analytically solved by introducing new parameters that represent the redundancy, and then, the redundancy parameters are determined based on some criteria. One of the advantages of these methods is that a closed-form inverse kinematic solution is given in terms of joint displacements rather than joint velocities. Hence, these methods guarantee absolute position accuracy as well as repeatability in trajectory tracking.

When a 7 DOF redundant manipulator is employed for fine manipulation tasks like assembly tasks, positioning accuracy has to be guaranteed. For this purpose, we need to resolve the redundancy in the position domain rather than the velocity domain. However, the existing position-based redundancy resolution methods can not deal with the problem of *joint limits*. The joint limits are not only mechanical limits but software limits for preventing collisions with external objects. This is usual for manipulators mounted on a mobile platform like a humanoid robot, where collisions with the body could occur. In such a case, not all redundancy resolutions are realizable due to the joint limits. Therefore, the effects of the joint limits have to be taken into account when resolving the redundancy.

Researches addressing the issue of joint limits in the position domain are rare. Lück and Lee [8] studied the topology of self-motion in the configuration space constrained by joint limits. Although this work supplies useful information regarding to the topological properties of self-motion, how to resolve the redundancy under joint limits is not addressed.

The objective of this paper is to develop a practical redundancy resolution method for 7 DOF redundant manipulators with joint limits. The distinction of our method is that the method analytically resolves the redundancy in the global configuration space under the joint limits. This approach brings the advantages that the positioning accuracy is guaranteed in principle and all the feasible solutions are obtainable with a light computational load.

This paper is organized in the following manner. Section II derives a parameterized inverse kinematic solution for a 7 DOF manipulator model. Section III identifies the feasible solutions under joint limits. Section IV develops an analytical redundancy resolution method for avoiding the joint limits. Finally, section V presents kinematic simulations to show that the proposed method is effective for avoiding the joint limits.

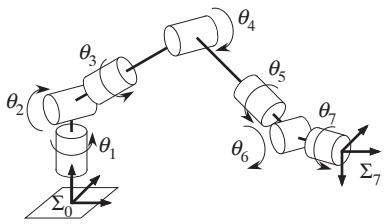

Fig. 1 7 DOF manipulator model.

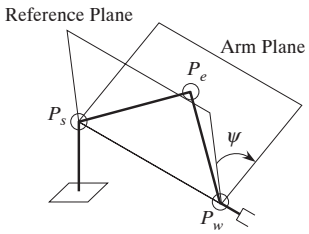

Fig. 2 Definition of arm angle ψ.

II. Parameterized Inverse Kinematics

This section provides an analytical inverse kinematic solution for a 7 DOF manipulator model. First, the manipulator model assumed in this paper is described. Next, a parameter is introduced to represent the redundancy. Then, the inverse kinematic solution is derived using the redundancy parameter.

A. Manipulator Model

In this paper, a S-R-S manipulator model is assumed. Namely, as shown in Fig. 1, the manipulator is assumed to have seven revolute joints, comprising three shoulder joints, one elbow joint, and three wrist joints.

To describe the kinematic relation between the joint angles and the pose (position and orientation) of the manipulator's tip, let us define joint coordinate systems. In this paper, each coordinate system Σ_i $(i = 0, 1, \cdots, 7)$ is determined based on the Denavit-Hartenberg rules [9]. The base coordinate system Σ_0 and the tip one Σ_7 are placed as shown in Fig. 1. With these coordinate systems, the Denavit-Hartenberg parameters are described as listed in Table 1. Note that the notation of the parameters is not unique because the parameters depend on the definition of the joint coordinate frames.

B. Redundancy Parameter

Since the tip pose is uniquely described by six parameters, an additional parameter is required to specify the manipulator's posture uniquely. This parameter is associated with a *self-motion* of the manipulator. To describe the self-motion, this paper incorporates the parameter termed *arm angle* [10]. As shown in Fig. 2, the arm angle ψ is defined as the angle between a reference plane and the arm plane spanned by the shoulder, elbow, and wrist.

In this paper, the reference plane is determined in the following way. The S-R-S manipulator can be regarded as a non-redundant manipulator when the joint angle 3 is fixed to zero. In this case, the arm plane is uniquely determined for a specified tip pose because no self-motion is possible for the virtual non-redundant manipulator. Since the arm plane is always deterministic except for the case of shoulder/elbow singularity, it can be used as the reference plane. We will refer the arm plane determined by the virtual non-redundant manipulator as the reference plane in the following.

Table 1 D-H parameters of 7 DOF manipulator model.

i	θ_i	α_i(rad)	d_i	a_i
1	θ_1	$-\pi/2$	d_{bs}	0
2	θ_2	$\pi/2$	0	0
3	θ_3	$-\pi/2$	d_{se}	0
4	θ_4	$\pi/2$	0	0
5	θ_5	$-\pi/2$	d_{ew}	0
6	θ_6	$\pi/2$	0	0
7	θ_7	0	d_{wt}	0

C. Derivation of Parameterized Inverse Kinematic Solution

Now, the inverse kinematic problem is solved using the arm angle. First, the forward kinematic relation incorporating the arm angle is formulated. Then, the inverse analysis is carried out to get the joint angles parameterized by the arm angle.

1) Forward Kinematic Analysis: The manipulator's tip pose is represented by the combination of the position ${}^0x_7 \in \Re^3$ and orientation ${}^0\boldsymbol{R}_7 \in SO(3)$ of the tip coordinate system viewed from the base one. The conventional forward kinematic analysis provides the kinematic relation between the tip pose and joint angles;

$$ {}^0\boldsymbol{x}_7 = {}^0\boldsymbol{l}_{bs} + {}^0\boldsymbol{R}_3 \left\{ {}^3\boldsymbol{l}_{se} + {}^3\boldsymbol{R}_4 \left({}^4\boldsymbol{l}_{ew} + {}^4\boldsymbol{R}_7 {}^7\boldsymbol{l}_{wt} \right) \right\}, \quad (1) $$

$$ {}^0\boldsymbol{R}_7 = {}^0\boldsymbol{R}_3 {}^3\boldsymbol{R}_4 {}^4\boldsymbol{R}_7, \quad (2) $$

where the superscript on the left side of each vector/matrix denotes the reference coordinate system, thus, ${}^i\boldsymbol{R}_j$ represents the orientation of the coordinate system j viewed from the coordinate system i, and ${}^0\boldsymbol{l}_{bs}$, ${}^3\boldsymbol{l}_{se}$, ${}^4\boldsymbol{l}_{ew}$, and ${}^7\boldsymbol{l}_{wt}$ are constant vectors given by

$$ {}^0\boldsymbol{l}_{bs} = \begin{bmatrix} 0 & 0 & d_{bs} \end{bmatrix}^T, $$
$$ {}^3\boldsymbol{l}_{se} = \begin{bmatrix} 0 & -d_{se} & 0 \end{bmatrix}^T, $$
$$ {}^4\boldsymbol{l}_{ew} = \begin{bmatrix} 0 & 0 & d_{ew} \end{bmatrix}^T, $$
$$ {}^7\boldsymbol{l}_{wt} = \begin{bmatrix} 0 & 0 & d_{wt} \end{bmatrix}^T. $$

The rotation matrix between the coordinate systems $i-1$ and i is given by

$$ {}^{i-1}\boldsymbol{R}_i = \begin{bmatrix} \cos\theta_i & -\sin\theta_i \cos\alpha_i & \sin\theta_i \sin\alpha_i \\ \sin\theta_i & \cos\theta_i \cos\alpha_i & -\cos\theta_i \sin\alpha_i \\ 0 & \sin\alpha_i & \cos\alpha_i \end{bmatrix} \quad (3) $$

Suppose that the desired tip pose is specified as ${}^0\boldsymbol{x}_7^d$ and ${}^0\boldsymbol{R}_7^d$. In this case, the shoulder-wrist axis must be fixed in

order to satisfy the specified tip pose, because the vector from the shoulder to the wrist, denoted by ${}^0\boldsymbol{x}_{sw}$, is given by

$$ {}^0\boldsymbol{x}_{sw} = {}^0\boldsymbol{x}_7^d - {}^0\boldsymbol{l}_{bs} - {}^0\boldsymbol{R}_7^d\, {}^7\boldsymbol{l}_{wt}. \tag{4} $$

Since the self-motion parameterized by the arm angle ψ is a rotation around this fixed axis, the self-motion does not affect the wrist position but does affect the wrist orientation. The orientational difference between the arm plane and the reference one is described [11] by

$$ {}^0\boldsymbol{R}_\psi = \boldsymbol{I}_3 + \sin\psi \left[{}^0\boldsymbol{u}_{sw}\times\right] + (1-\cos\psi)\left[{}^0\boldsymbol{u}_{sw}\times\right]^2, \tag{5} $$

where $\boldsymbol{I}_3 \in \Re^{3\times3}$ is the identity matrix, ${}^0\boldsymbol{u}_{sw} \in \Re^3$ is the unit vector of ${}^0\boldsymbol{x}_{sw}$, and $\left[{}^0\boldsymbol{u}_{sw}\times\right]$ denotes the skew-symmetric matrix of the vector ${}^0\boldsymbol{u}_{sw}$. Thus, the wrist orientation is described by

$$ {}^0\boldsymbol{R}_4 = {}^0\boldsymbol{R}_\psi\, {}^0\boldsymbol{R}_4^o, \tag{6} $$

where ${}^0\boldsymbol{R}_4^o$ represents the wrist orientation when the arm plane coincides with the reference plane.

As Fig. 2 implies, the elbow angle (joint 4) depends only on the wrist position and is not subject to the arm angle. It follows that ${}^3\boldsymbol{R}_4$ and ${}^3\boldsymbol{R}_4^o$ are same. Therefore, (6) can be simplified to

$$ {}^0\boldsymbol{R}_3 = {}^0\boldsymbol{R}_\psi\, {}^0\boldsymbol{R}_3^o. \tag{7} $$

Substituting (7) into (1) and (2), we can get the kinematic relation including the arm angle parameter.

2) Inverse Kinematic Analysis: First, the elbow joint angle is computed. Substituting (1) into (4), we have

$$ {}^0\boldsymbol{x}_{sw} = {}^0\boldsymbol{R}_3 \left({}^3\boldsymbol{l}_{se} + {}^3\boldsymbol{R}_4\, {}^4\boldsymbol{l}_{ew}\right). \tag{8} $$

Computing the square sum of the norm of ${}^0\boldsymbol{x}_{sw}$, we get

$$ \left\|{}^0\boldsymbol{x}_{sw}\right\|^2 = d_{se}^2 + d_{ew}^2 + 2d_{se}d_{ew}\cos\theta_4. \tag{9} $$

The joint angle θ_4 can be derived from this equation.

Second, the shoulder joint angles when $\psi = 0$ are computed to determine the reference plane. As mentioned before, the reference plane is equivalent to the arm plane when the joint angle θ_3 is fixed to zero. Substituting (7) and $\theta_3 = 0$ into (8), we have

$$ {}^0\boldsymbol{x}_{sw} = {}^0\boldsymbol{R}_1^o\, {}^1\boldsymbol{R}_2^o\, {}^2\boldsymbol{R}_3\big|_{\theta_3=0} \left({}^3\boldsymbol{l}_{se} + {}^3\boldsymbol{R}_4\, {}^4\boldsymbol{l}_{ew}\right). \tag{10} $$

Since the joint angle θ_4 is given by (9), unknown parameters in (10) are θ_1^o and θ_2^o only. Comparing both sides of (10), we can get unique solutions of θ_1^o and θ_2^o.

Third, the shoulder joint angles for an arm angle ψ are computed. Substituting (5) into (7), we have

$$ {}^0\boldsymbol{R}_3 = \boldsymbol{A}_s \sin\psi + \boldsymbol{B}_s \cos\psi + \boldsymbol{C}_s, \tag{11} $$

where $\boldsymbol{A}_s$, $\boldsymbol{B}_s$, and $\boldsymbol{C}_s$ are constant matrices given by

$$ \begin{aligned} \boldsymbol{A}_s &= \left[{}^0\boldsymbol{u}_{sw}\times\right] \cdot {}^0\boldsymbol{R}_3^o, \\ \boldsymbol{B}_s &= -\left[{}^0\boldsymbol{u}_{sw}\times\right]^2 \cdot {}^0\boldsymbol{R}_3^o, \\ \boldsymbol{C}_s &= \left[{}^0\boldsymbol{u}_{sw}\, {}^0\boldsymbol{u}_{sw}^T\right] \cdot {}^0\boldsymbol{R}_3^o. \end{aligned} $$

Computing the rotation matrix ${}^0\boldsymbol{R}_3$ and combining some elements of the matrix, we can get the following equations;

$$ \tan\theta_1 = \frac{-a_{s22}\sin\psi - b_{s22}\cos\psi - c_{s22}}{-a_{s12}\sin\psi - b_{s12}\cos\psi - c_{s12}}, \tag{12} $$

$$ \cos\theta_2 = -a_{s32}\sin\psi - b_{s32}\cos\psi - c_{s32}, \tag{13} $$

$$ \tan\theta_3 = \frac{a_{s33}\sin\psi + b_{s33}\cos\psi + c_{s33}}{-a_{s31}\sin\psi - b_{s31}\cos\psi - c_{s31}}, \tag{14} $$

where a_{sij}, b_{sij}, and c_{sij} are the (i,j) element of the matrices $\boldsymbol{A}_s$, $\boldsymbol{B}_s$, and $\boldsymbol{C}_s$, respectively. The joint angles θ_1, θ_2, and θ_3 can be derived from these equations.

Lastly, the wrist joint angles are computed. Substituting (7) into (2), we have

$$ {}^4\boldsymbol{R}_7 = \boldsymbol{A}_w \sin\psi + \boldsymbol{B}_w \cos\psi + \boldsymbol{C}_w, \tag{15} $$

where $\boldsymbol{A}_w$, $\boldsymbol{B}_w$, and $\boldsymbol{C}_w$ are constant matrices given by

$$ \begin{aligned} \boldsymbol{A}_w &= -{}^3\boldsymbol{R}_4^T \cdot {}^0\boldsymbol{R}_3^{oT} \cdot \left[{}^0\boldsymbol{u}_{sw}\times\right] \cdot {}^0\boldsymbol{R}_7^d, \\ \boldsymbol{B}_w &= -{}^3\boldsymbol{R}_4^T \cdot {}^0\boldsymbol{R}_3^{oT} \cdot \left[{}^0\boldsymbol{u}_{sw}\times\right]^2 \cdot {}^0\boldsymbol{R}_7^d, \\ \boldsymbol{C}_w &= {}^3\boldsymbol{R}_4^T \cdot {}^0\boldsymbol{R}_3^{oT} \cdot \left[{}^0\boldsymbol{u}_{sw}\, {}^0\boldsymbol{u}_{sw}^T\right] \cdot {}^0\boldsymbol{R}_7^d. \end{aligned} $$

Computing the rotation matrix ${}^4\boldsymbol{R}_7$ and combining some elements of the matrix, we can get the following equations;

$$ \tan\theta_5 = \frac{a_{w23}\sin\psi + b_{w23}\cos\psi + c_{w23}}{a_{w13}\sin\psi + b_{w13}\cos\psi + c_{w13}}, \tag{16} $$

$$ \cos\theta_6 = a_{w33}\sin\psi + b_{w33}\cos\psi + c_{w33}, \tag{17} $$

$$ \tan\theta_7 = \frac{a_{w32}\sin\psi + b_{w32}\cos\psi + c_{w32}}{-a_{w31}\sin\psi - b_{w31}\cos\psi - c_{w31}}. \tag{18} $$

The joint angles θ_5, θ_6, and θ_7 can be derived from these equations.

III. Feasible Inverse Kinematic Solutions under Joint Limits

This section investigates feasible inverse kinematic solutions under joint limits. First, the relationship between the arm angle and the joint angles is analyzed. The feasible region of the arm angle is then identified for a specified tip pose.

A. Relationship between Arm Angle and Joint Angles

As described in the previous section, the joint angles depend on the arm angle even if the tip pose is fixed. Here, let us examine how the joint angles vary with the arm angle for a fixed tip pose.

As shown in (9), the elbow joint is independent on the arm angle, while the others are subject to the arm angle. The relationships between the arm angle and the joint angles are represented by (12)-(14) and (16)-(18). In each of the equations, the tangent or cosine of a joint angle is related to a function of the arm angle. Therefore, it is enough to investigate only the two function types in order to know the characteristics of all the joint angles. Below, the relationship between an arm angle and a joint angle for each function type is explored.

1) Tangent Type: Suppose that a joint angle θ_i is given by

$$\tan\theta_i = \frac{a_n \sin\psi + b_n \cos\psi + c_n}{a_d \sin\psi + b_d \cos\psi + c_d}.$$

Differentiating both sides with respect to ψ, we can get

$$\frac{d\theta_i}{d\psi} = \frac{a_t \mathrm{s}\psi + b_t \mathrm{c}\psi + c_t}{\left(a_n \mathrm{s}\psi + b_n \mathrm{c}\psi + c_n\right)^2 + \left(a_d \mathrm{s}\psi + b_d \mathrm{c}\psi + c_d\right)^2}, \tag{19}$$

where s_ψ and c_ψ denote $\sin\psi$ and $\cos\psi$, respectively, and

$$\begin{aligned} a_t &= b_d c_n - b_n c_d, \\ b_t &= a_n c_d - a_d c_n, \\ c_t &= a_n b_d - a_d b_n. \end{aligned}$$

Since the denominator in (19) is always positive or zero, the sign of the gradient of θ_i against ψ is determined by the sign of the numerator. Functional analysis of the numerator shows that the sign of the numerator changes if the condition

$$a_t^2 + b_t^2 - c_t^2 > 0. \tag{20}$$

is satisfied. In this case, there exist the arm angles ψ_0 where the numerator is zero, which are described by

$$\psi_0 = 2\tan^{-1}\frac{a_t \pm \sqrt{a_t^2 + b_t^2 - c_t^2}}{b_t - c_t}. \tag{21}$$

Since the sign of the gradient changes at ψ_0, θ_i is minimized or maximized locally at ψ_0. Since the second order differential coefficient of θ_i at ψ_0 can be computed by

$$\left.\frac{d^2\theta_i}{d\psi^2}\right|_{\psi_0} = \frac{-b_t \mathrm{s}\psi_0 + a_t \mathrm{c}\psi_0}{\left(a_n \mathrm{s}\psi_0 + b_n \mathrm{c}\psi_0 + c_n\right)^2 + \left(a_d \mathrm{s}\psi_0 + b_d \mathrm{c}\psi_0 + c_d\right)^2}, \tag{22}$$

we can distinguish between the minimum and the maximum by evaluating the sign of the coefficient. Although the details are omitted here due to the paper limit, further analysis shows that only two distinct ψ_0 are possible, one of which globally minimizes θ_i and the other globally maximizes θ_i.

As a consequence, the relationship between θ_i and ψ is classified into either of the following two cases;

(1) Case with the global minimum and maximum:
If the condition (20) is satisfied, there always exist the global minimum and maximum, but neither local minima nor local maxima exist. The arm angles associated with the global minimum and maximum are given by (21). The joint angle θ_i with respect to the arm angle ψ is plotted as shown in Fig. 3 (a).

(2) Case with no minima and maxima:
If the condition (20) is not satisfied, the sign of the gradient given by (19) is always same for any ψ. This indicates that θ_i monotonically increases/decreases as ψ varies. The joint angle θ_i with respect to the arm angle ψ is plotted as shown in Fig. 3 (b).

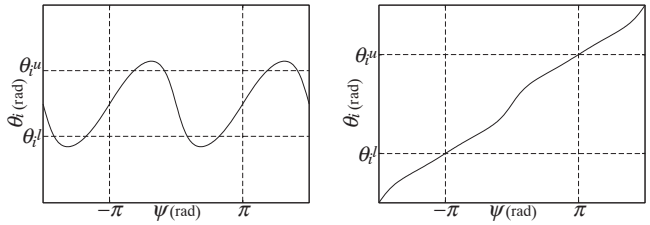

(a) Case 1 (b) Case 2

Fig. 3 Profile of joint angle θ_i with respect to arm angle ψ when θ_i is given by the tangent function; (a) Case with global minimum and maximum, and (b) Case with no minima/maxima.

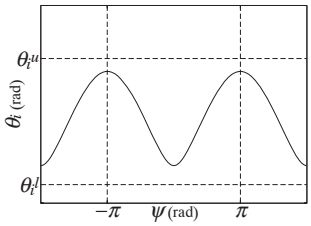

Fig. 4 Profile of joint angle θ_i with respect to arm angle ψ when θ_i is given by the cosine function.

2) Cosine Type: Suppose that a joint angle θ_i is given by

$$\cos\theta_i = a\sin\psi + b\cos\psi + c.$$

Differentiating both sides with respect to ψ, we get

$$\frac{d\theta_i}{d\psi} = -\frac{1}{\sin\theta_i}\left(a\cos\psi - b\sin\psi\right). \tag{23}$$

Computing the arm angle ψ_0, which makes (23) zero, yields

$$\psi_0 = \tan^{-1}\frac{a}{b}. \tag{24}$$

It can be verified that there always exist two distinct ψ_0, which are π radian apart. Since the second order differential coefficient at $\psi_0 \pm \pi$ ensures that

$$\sin\theta_i\left(\psi_0 \pm \pi\right) \cdot \left.\frac{d^2\theta_i}{d\psi^2}\right|_{\psi_0 \pm \pi} = -\sin\theta_i\left(\psi_0\right) \cdot \left.\frac{d^2\theta_i}{d\psi^2}\right|_{\psi_0},$$

if the signs of θ_i at ψ_0 and $\psi_0 \pm \pi$ are same, θ_i is globally minimized at one of the two arm angles and maximized at the other. Consequently, the joint angle θ_i with respect to the arm angle ψ is plotted as shown in Fig. 4.

B. Feasible Region of Arm Angle

Now, the feasible region of the arm angle under joint limits is identified. In the following, assume that joint limits are represented by

$$\theta_i^l \le \theta_i \le \theta_i^u, \ \ (i = 1, 2, \cdots, 7) \tag{25}$$

where θ_i^l and θ_i^u are the lower and upper bounds of the joint angle θ_i, respectively.

As shown above, the profile of a joint angle with respect to the arm angle is classified into either of the two types, one

of which involves the global minimum and maximum, while the other involves no minima/maxima. In the latter case, as shown in Fig. 3 (b), the joint angle will inevitably reach to its joint limit when the arm angle is going to increase/decrease. Therefore, when a joint angle involves no minima/maxima, the feasible region of the arm angle is given by the single domain, which is bounded by the two arm angles corresponding to the upper and lower bounds of the joint angle.

On the other hand, when a joint angle involves the global minimum and maximum, the feasible region is somewhat complex. Let ψ_0^{min} and ψ_0^{max} be the arm angles that minimizes and maximizes the joint angle, respectively. Also, let θ_i^{min} and θ_i^{max} be the joint angles corresponding to ψ_0^{min} and ψ_0^{max}, respectively. Taking into account the profile of the joint angle, we can find that the following five cases are possible. Note that the width of the range of the arm angle is limited to 2π radian in the following, but this does not lose generality because the arm angle forms a *torus* [12].

(1) $\theta_i^{min} > \theta_i^u$ or $\theta_i^{max} < \theta_i^l$:
No feasible region of the arm angle exists.

(2) $\theta_i^{min} < \theta_i^l$ and $\theta_i^l \leq \theta_i^{max} \leq \theta_i^u$:
Since ψ_0^{max} is feasible but ψ_0^{min} is not, a certain region including the point ψ_0^{max} is feasible. The boundaries of the region is given by solving the equation $\theta_i(\psi) = \theta_i^l$.

(3) $\theta_i^l \leq \theta_i^{min} \leq \theta_i^u$ and $\theta_i^{max} > \theta_i^u$:
Since ψ_0^{min} is feasible but ψ_0^{max} is not, a certain region including the point ψ_0^{min} is feasible. The boundaries of the region is given by solving the equation $\theta_i(\psi) = \theta_i^u$.

(4) $\theta_i^{min} < \theta_i^l$ and $\theta_i^{max} > \theta_i^u$:
Since both ψ_0^{min} and ψ_0^{max} are infeasible but somewhere in between the two points is feasible, the feasible region is given by excluding two regions, which includes ψ_0^{min} and ψ_0 respectively, from the entire domain of the arm angle. The boundaries of the infeasible regions are given by solving the equations $\theta_i(\psi) = \theta_i^l$ and $\theta_i(\psi) = \theta_i^u$.

(5) $\theta_i^l \leq \theta_i^{min} \leq \theta_i^u$ and $\theta_i^l \leq \theta_i^{max} \leq \theta_i^u$:
The entire domain is feasible.

Except for (1), the feasible region of the arm angle for a single joint is composed of one or more closed subregions. Therefore, the feasible region of the arm angle for the joint i, denoted by Ψ_i, is represented by

$$\Psi_i = \bigcup_{j=1}^{n_i} \Psi_{ij}, \tag{26}$$

where Ψ_{ij} is a closed subregion, and n_i is the number of the subregions. As a consequence, the feasible region Ψ satisfying all the joint limits is represented by

$$\Psi = \bigcap_{i=1}^{7} \Psi_i. \tag{27}$$

IV. Redundancy Resolution

This section develops a practical redundancy resolution for a S-R-S manipulator with joint limits. The joint limits directly affect the reachable region of the manipulator's tip. Since the joint angles depend on the arm angle, the reachable region would be smaller than the kinematic one if the arm angle is ill-chosen. To elicit the maximal performance of the manipulator, the arm angle should be determined to avoid the joint limits as much as possible. Below, we discuss how the arm angle should be determined to avoid the joint limits.

A. Approach

Since the shoulder and wrist joint angles depend on the arm angle, the joint limits of the shoulder and wrist portions may be avoidable by regulating the arm angle properly. Each of the portions consists of three revolute joints and all the three joint axes intersect at a single point. This simple mechanism enables us to regard each portion as a virtual spherical joint. Since a spherical displacement can be described by a rotation around an axis [11], the rotation angle ϕ is one of the indices that characterize the spherical displacement.

Let ϕ_d be the rotation angle where the three joints are at designated angles. It is expected that the orientational displacement of the spherical joint will get closest to the designated one when $\phi = \phi_d$. If each of the designated joint angles is selected as the angle furthest from its limits, the joint limits will be avoided as much as possible by finding ϕ nearest to ϕ_d. Based on this theory, we will develop three methods to avoid the joint limits associated with the shoulder portion, the wrist portion, and the combination of them, respectively.

B. Joint Limit Avoidance for Shoulder Joints

First, the arm angle is derived to avoid the shoulder joint limits. Let θ_1^d, θ_2^d, and θ_3^d be the desired angles of θ_1, θ_2, and θ_3 respectively, and ${}^0\boldsymbol{R}_3^d$ be the orientation at the desired angles. The difference between the desired and actual orientations is described by

$${}^0\boldsymbol{R}_3 \cdot {}^0\boldsymbol{R}_3^{dT} = \boldsymbol{I}_3 + \sin\phi_s \left[{}^0\boldsymbol{u}_s\times\right] + (1-\cos\phi_s)\left[{}^0\boldsymbol{u}_s\times\right]^2, \tag{28}$$

where $\boldsymbol{u}_s \in \Re^3$ and $\phi_s \geq 0$ are the unit vector of the rotation axis and the rotation angle around the axis, respectively. Since ϕ_s becomes zero when the actual orientation coincides with the desired one, ϕ_s has to be minimized to make the actual orientation closest to the desired one.

Substituting (11) into (28) and computing its trace, we have

$$\begin{aligned}&\text{trace}\left({}^0\boldsymbol{R}_3 \cdot {}^0\boldsymbol{R}_3^{dT}\right)\\ &= a_s\sin\psi + b_s\cos\psi + c_s\\ &= 1 + 2\cos\phi_s,\end{aligned}$$

where $a_s = \text{trace}\left(\boldsymbol{A}_s \cdot {}^0\boldsymbol{R}_3^{dT}\right)$, $b_s = \text{trace}\left(\boldsymbol{B}_s \cdot {}^0\boldsymbol{R}_3^{dT}\right)$, and $c_s = \text{trace}\left(\boldsymbol{C}_s \cdot {}^0\boldsymbol{R}_3^{dT}\right)$. Thus, the problem of minimizing ϕ_s is reduced to that of maximizing the objective function

$$f_s(\psi) = a_s\sin\psi + b_s\cos\psi + c_s.$$

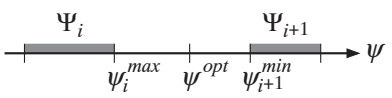

Fig. 5 The optimal arm angle is not always feasible under joint limits.

It can be verified that $f_s(\psi)$ is minimized or maximized at

$$\psi_s = \tan^{-1}\frac{a_s}{b_s}. \tag{29}$$

Let ψ_s^{opt} be the solution that maximizes f_s. Then, another solution is given by $\psi_s^{opt} \pm \pi$, which minimizes f_s. Thus, the optimal arm angle for avoiding the shoulder joint limits is given by ψ_s^{opt}.

If this solution is infeasible due to the joint limits, we have to modify the solution. In general, the feasible region of the arm angle consists of one or more closed subregions. When ψ_s^{opt} is infeasible, there exist two subregions Ψ_i and Ψ_{i+1} enclosing the infeasible point as shown in Fig. 5. Let ψ_i^{max} be the boundary of the subregion Ψ_i, which is closer to ψ_s^{opt}. Similarly, let ψ_{i+1}^{min} be the boundary of the subregion Ψ_{i+1}, which closer to ψ_s^{opt}. Since the objective function f_s monotonically increases within the range $[\psi_s^{opt} - \pi,\ \psi_s^{opt}]$ and monotonically decreases within the range $[\psi_s^{opt},\ \psi_s^{opt} + \pi]$, the optimal and feasible arm angle is either ψ_i^{max} or ψ_{i+1}^{min}, which is closer to ψ_s^{opt}.

C. Joint Limit Avoidance for Wrist Joints

The arm angle for avoiding the wrist joint limits can be derived in the similar way. In this case, the objective function is obtained from (15) as

$$f_w(\psi) = a_w \sin\psi + b_w \cos\psi + c_w,$$

where $a_w = \text{trace}\left(\boldsymbol{A}_w \cdot {}^4\boldsymbol{R}_7^{dT}\right)$, $b_w = \text{trace}\left(\boldsymbol{B}_w \cdot {}^4\boldsymbol{R}_7^{dT}\right)$, and $c_w = \text{trace}\left(\boldsymbol{C}_w \cdot {}^4\boldsymbol{R}_7^{dT}\right)$, and ${}^4\boldsymbol{R}_7^d$ is the desired orientation of the wrist three joints. This function is minimized or maximized at

$$\psi_w = \tan^{-1}\frac{a_w}{b_w}. \tag{30}$$

Let ψ_w^{opt} be the solution that maximizes f_w. If it is feasible under the joint limits, it is the optimal arm angle for avoiding the wrist joint limits. Otherwise, the optimal arm angle is the one which is feasible and closest to ψ_w^{opt}.

D. Joint Limit Avoidance for All Joints

Now, how to avoid all the joint limits is discussed. As mentioned above, the elbow joint limits are not avoidable by regulating the arm angle, while the shoulder and wrist joint limits are avoidable by maximizing the function f_s and f_w, respectively. Hence, it is expected that both the shoulder and wrist joint limits will be avoided together by maximizing an objective function combined with f_s and f_w. A candidate of such functions is, for example,

$$f(\psi) = \frac{r_s f_s(\psi) + r_w f_w(\psi)}{r_s + r_w},$$

Table 2 Upper and lower bounds of each joint (unit: degree)

i	1	2	3	4	5	6	7
θ_i^u	90	45	120	135	90	90	120
θ_i^l	-90	-45	-120	0	-90	-90	-120

where $r_s \geq 0$ and $r_w \geq 0$ are weighting factors. This function is minimized or maximized at

$$\psi = \tan^{-1}\frac{r_s a_s + r_w a_w}{r_s b_s + r_w b_w}. \tag{31}$$

Consequently, the optimal arm angle is given by the solution ψ^{opt} that maximizes f, if it is feasible. Otherwise, the optimal arm angle is the one which is feasible and closest to ψ^{opt}.

V. Simulation

This section performs kinematic simulations to show the effectiveness of the methods developed in this paper. The kinematic parameters listed in Table 1 are used in the simulations, where each link length is set to $d_{bs} = 0.317$ (m), $d_{se} = 0.45$ (m), $d_{ew} = 0.48$ (m), $d_{wt} = 0.07$ (m). Besides, the movable range of each joint is limited as shown in Table 2.

Suppose that the desired tip pose is given by

$$\boldsymbol{x}_d = \begin{bmatrix} 0.65 & 0 & 0.5 \end{bmatrix}^T \text{ (m)},$$
$$\boldsymbol{R}_d = \begin{bmatrix} -1 & 0 & 0 \\ 0 & 1 & 0 \\ 0 & 0 & -1 \end{bmatrix}. \tag{32}$$

The feasible region of the arm angle can be computed by the method presented in section III. The feasible region for each joint angle is obtained as

$$\Psi_1 = [-180,\ 180] \text{ (deg)},$$
$$\Psi_2 = [-45.991,\ 45.991] \text{ (deg)},$$
$$\Psi_3 = [-111.734,\ 111.734] \text{ (deg)},$$
$$\Psi_5 = [-108.926,\ 108.926] \text{ (deg)},$$
$$\Psi_6 = [-62.154,\ 62.154] \text{ (deg)},$$
$$\Psi_7 = [-180,\ 180] \text{ (deg)},$$

where the range of the arm angle is $[-180,\ 180]$ (deg). The feasible region of the arm angle for all the joints is the intersection of these regions, which is given by

$$\Psi = [-45.991,\ 45.991] \text{ (deg)}.$$

Computing the joint angles at the minimal and maximal arm angles in order to validate this result, we obtain

$$\boldsymbol{\theta}|_{\psi^{min}} = [43.992,\ 45,\ -71.419,\ 82.872,\ 42.572,\ 82.193,\ -27.693]^T \text{ (deg)},$$
$$\boldsymbol{\theta}|_{\psi^{max}} = [-43.992,\ 45,\ 71.419,\ 82.872,\ -42.572,\ 82.193,\ 27.693]^T \text{ (deg)}.$$

Since the joint 2 has reached to its limit at both of the arm angles, the arm angle can not go beyond these values.

Next, suppose that the tip pose is specified by

$$\boldsymbol{x}_d = \begin{bmatrix} 0.65 & 0 & 0.5 \end{bmatrix}^T \text{ (m)},$$
$$\boldsymbol{R}_d = \begin{bmatrix} 0 & -1 & 0 \\ -1 & 0 & 0 \\ 0 & 0 & -1 \end{bmatrix}.$$

In this case, the feasible region of the arm angle is computed as $\Psi = [-43.246,\ 43.246]$ (deg). The optimal arm angles for avoiding the shoulder, wrist, and all joint limits are given by (29), (30), and (31), respectively. Computing them, we have $\psi_s^{opt} = 0$ (deg), $\psi_w^{opt} = 54.479$ (deg), $\psi^{opt} = 25.017$ (deg), where the weighting factors in (31) are $r_s = r_w = 0.5$. Since ψ_w^{opt} is infeasible, it has to be modified into the nearest feasible value $\psi_w^{opt} = 43.246$ (deg). To validate the results, computing the joint angles at $\psi = 0$ and $\psi = \psi^{opt}$, we obtain

$$\begin{aligned} \boldsymbol{\theta}|_{\psi=0} &= [0,\ 25.666,\ 0,\ 82.872, \\ &\qquad 0,\ 71.463,\ -90]^T \text{ (deg)}, \\ \boldsymbol{\theta}|_{\psi=\psi^{opt}} &= [-32.325,\ 32.687,\ 46.864,\ 82.872, \\ &\qquad -24.101,\ 74.814,\ -73.709]^T \text{ (deg)}. \end{aligned}$$

As shown, the absolute value of the maximal joint angle at $\psi = 0$ is $|\theta_7| = 90$, while the one at $\psi = \psi^{opt}$ is reduced to $|\theta_6| = 74.814$. Thus, the redundancy resolution method is effective for keeping the joint angles away from the limits.

Lastly, let us investigate how the redundancy resolution affects the reachable region of the manipulator's tip. As an example, suppose that the tip rotates around z-axis in the absolute coordinate system without changing the tip position, where the initial pose is given by (32). Then, the tip pose can be described by

$$\boldsymbol{x}_d = \begin{bmatrix} 0.65 & 0.0 & 0.5 \end{bmatrix}^T \text{ (m)},$$
$$\boldsymbol{R}_d = \begin{bmatrix} -\cos\gamma & -\sin\gamma & 0 \\ -\sin\gamma & \cos\gamma & 0 \\ 0 & 0 & -1 \end{bmatrix},$$

where γ represents the rotation angle around the z-axis. When γ increases/decreases continuously, the tip rotates around the z-axis, and eventually reaches its limit at some point. Thus, the reachable region of the tip is equivalent to the feasible range of the rotation angle γ.

When the arm angle is fixed to zero, i.e. $\psi = 0$, the reachable region is given by

$$\Gamma_0 = [-120,\ 120] \text{ (deg)}.$$

For comparison, consider that the arm angle is controlled to satisfy the arm angle given by (31) for avoiding all the joint limits, i.e. $\psi = \psi^{opt}$. Computing the reachable region, we have

$$\Gamma = [-147.693,\ 147.693] \text{ (deg)}.$$

These results indicate that the redundancy resolution method is indeed effective for expanding the reachable region.

VI. Concluding Remarks

This paper proposed a practical redundancy resolution for 7 DOF redundant manipulators with joint limits. First, a parameterized inverse kinematic solution in the position domain was derived using the arm angle parameter. Second, feasible inverse kinematic solutions under joint limits were identified. Then, an analytical redundancy resolution method for avoiding the joint limits was developed. Lastly, kinematic simulations showed that the redundancy resolution method was effective for avoiding the joint limits as well as expanding the reachable region of the manipulator's tip.

We have successfully applied this redundancy resolution method to an anthropomorphic arm of a humanoid robot, where the joint movable ranges are severely limited. Our objective is to execute various practical tasks like assembly tasks by the humanoid robot. To deal with environmental uncertainties, we have adopted a position-based impedance control scheme, which requires a position-based redundancy resolution. The proposed method has contributed immensely to achieving an assembly task by expanding the reachable region of the arm's tip despite the severe joint limits.

References

[1] D.N.Nenchev, "Redundancy Resolution through Local Optimization: A Review," *J. Robotic Systems*, vol.6, no.6, pp.769–798, 1989.

[2] T.Yoshikawa, "Manipulability and Redundancy Control of Robotic Mechanisms," *Proc. 1985 IEEE Int. Conf. Robotics and Automation*, pp.1004–1009, 1985.

[3] K.C.Suh and J.M.Hollerbach, "Local versus Global Torque Optimization of Redundant Manipulators," *Proc. 1987 IEEE Int. Conf. Robotics and Automation*, pp.619–624, 1987.

[4] Y.Nakamura, H.Hanafusa, and T.Yoshikawa, "Task-Priority Based Redundancy Control of Robot Manipulators," *Int. J. Robotics Research*, vol.6, no.2, pp.3–15, 1987.

[5] J.Nakanishi, R.Cory, M.Mistry, J.Peters, and S.Schaal, "Comparative Experiments on Task Space Control with Redundancy Resolution," *Proc. 2005 IEEE/RSJ Int. Conf. Intelligent Robots and Systems*, pp.1575–1582, 2005.

[6] S.Lee and A.K.Bejczy, "Redundant Arm Kinematic Control Based on Parameterization," *Proc. 1991 IEEE Int. Conf. Robotics and Automation*, pp.458–465, 1991.

[7] T.Asfour and R.Dillmann, "Human-like Motion of a Humanoid Robot Arm Based on a Closed-Form Solution of the Inverse Kinematics Problem," *Proc. 2003 IEEE/RSJ Int. Conf. Intelligent Robots and Systems*, pp.1407–1412, 2003.

[8] C.L.Lück and S.Lee, "Self-Motion Topology for Redundant Manipulators with Joint Limits," *Proc. 1993 IEEE/RSJ Int. Conf. Intelligent Robots and Systems*, pp.626–631, 1993.

[9] H.Asada and J.J.E.Slotine, *Robot Analysis and Control*, John Wiley & Sons, 1986.

[10] K.Kreutz-Delgado, M.Long, and H.Seraji, "Kinematic Analysis of 7-DOF Manipulators," *Int. J. Robotics Research*, vol.11, no.5, pp.469–481, 1992.

[11] J.M.McCarthy, *An Introduction to Theoretical Kinematics*, MIT Press, 1990.

[12] J.W.Burdick, "On the Inverse Kinematics of Redundant Manipulators: Characterization of the Self-Motion Manifolds," *Proc. 1989 IEEE Int. Conf. Robotics and Automation*, pp.264–270, 1989.